Genetically altered AMPA-type glutamate receptor kinetics in interneurons disrupt long-range synchrony of gamma oscillation

Elke C. Fuchs*, Helen Doheny[†‡], Howard Faulkner[‡], Antonio Caputi*, Roger D. Traub[§], Andrea Bibbig[§], Nancy Kopell[¶], Miles A. Whittington[†‡], and Hannah Monyer*[‖]

*Department of Clinical Neurobiology, University Hospital of Neurology, INF 364, Heidelberg, Germany; [‡]Imperial College School of Medicine, South Kensington, London SW7 2AZ, United Kingdom; [†]School of Biomedical Sciences, The Worsley Building, University of Leeds, Leeds LS2 9NL, United Kingdom; [§]Department of Pharmacology, Division of Neuroscience, University of Birmingham School of Medicine, Birmingham B15 2TT, United Kingdom; and [¶]Department of Mathematics, Boston University, Boston, MA 02215

Contributed by Nancy Kopell, December 28, 2000

Gamma oscillations synchronized between distant neuronal populations may be critical for binding together brain regions devoted to common processing tasks. Network modeling predicts that such synchrony depends in part on the fast time course of excitatory postsynaptic potentials (EPSPs) in interneurons, and that even moderate slowing of this time course will disrupt synchrony. We generated mice with slowed interneuron EPSPs by gene targeting, in which the gene encoding the 67-kDa form of glutamic acid decarboxylase (GAD67) was altered to drive expression of the α-amino-3-hydroxy-5-methyl-4-isoxazolepropionic acid (AMPA) glutamate receptor subunit GluR-B. GluR-B is a determinant of the relatively slow EPSPs in excitatory neurons and is normally expressed at low levels in γ-aminobutyric acid (GABA)ergic interneurons, but at high levels in the GAD-GluR-B mice. In both wild-type and GAD-GluR-B mice, tetanic stimuli evoked gamma oscillations that were indistinguishable in local field potential recordings. Remarkably, however, oscillation synchrony between spatially separated sites was severely disrupted in the mutant, in association with changes in interneuron firing patterns. The congruence between mouse and model suggests that the rapid time course of AMPA receptor-mediated EPSPs in interneurons might serve to allow gamma oscillations to synchronize over distance.

Gamma-frequency (30- to 90-Hz) neuronal oscillations, occurring in a non-time-locked fashion in response to visual stimuli, have been proposed to encode global features of spatially extended stimuli (1). A crucial physiological question concerns how synchrony arises, given the expected slow axonal conduction times in the cortex, estimated to be as low as 0.10–0.15 mm/ms (2, 3).

Network simulations (containing model pyramidal cells, interneurons, and axon conduction delays) predict that tight synchrony between distant sites could arise as an emergent property—without a central pacemaker—when interneurons fire in doublets (4–7). Precise timing of the doublet interval—determined in part by α-amino-3-hydroxy-5-methyl-4-isoxazolepropionic acid (AMPA)-receptor mediated excitation from pyramidal cells, especially cells at a distance from the postsynaptic interneuron—provides a signal encoding phase lags between separated neurons; this signal would provide feedback to nearby pyramidal cells, in the form of synaptic inhibition, which would tend to correct for phase differences (ref. 8; *Appendix,* which is published as supplemental data on the PNAS web site, www.pnas.org).

Here we use a combination of simulation, transgenic, and electrophysiological techniques to show that interneuron doublets are necessary for two-site synchrony to occur and that they critically depend on excitatory postsynaptic potential (EPSP) kinetics in interneurons.

Experimental Procedures

Simulations. Network simulations of gamma oscillations were performed by using the program described in Traub *et al.* (5). Briefly, the network consisted of a 96 × 32 cell array of pyramidal neurons, and a superimposed 4 × 32 array of interneurons, representing a 1.92-mm extent of CA1. Each neuron was modeled as a multicompartment object with soma, branching dendrites, and a segment of axon. Interneuron dendrites contained active conductances, as in Whittington *et al.* (ref. 9; see also ref. 10). AMPA and γ-aminobutyric acid $(GABA)_A$ receptor-mediated synaptic actions were simulated between the various cell types, and interneurons contacted (*i*) axon initial segment, (*ii*) the soma and proximal dendrites, or (*iii*) more distal dendrites. Pyramidal axon conduction velocity was 0.5 m/s, giving a 3.84-ms conduction delay across the array. Gamma oscillations were induced in the network by tonic excitatory conductances (reversal potential 60 mV positive to rest), developing in the dendrites of pyramidal neurons (55–60 nS) and of interneurons (5.0–5.2 nS) (6).

For analysis of the network effects of AMPA receptor-mediated synaptic conductances on interneurons, the unitary synaptic conductance was assumed to have the form Constant × $t \times \exp(-t/\tau)$ nS (t = time in ms), where the constant and τ were parameters. Baseline value of the constant was 2.0 and of that of τ was 1.0. Simulations were run in which one or the other of these values was altered, whereas other parameters (such as depolarizing conductances to pyramidal cells and interneurons, and other synaptic conductance time courses) were kept fixed. A unitary inhibitory postsynaptic current (IPSC) produced in an interneuron by a presynaptic basket cell had the form Constant × 2.0 × $\exp(-t/10)$ nS; a unitary IPSC produced in an interneuron by a presynaptic dendrite-contacting interneuron had the form Constant × 0.2 × $\exp(-t/50)$. For each simulation, the program stored somatic potentials of selected cells, and average potentials of groups of pyramidal cells, one group at either end of the array. Synchrony was analyzed by computing auto- and cross-correlations of these average signals. Simulations ran on an IBM SP2 parallel computer with 12 processors. For computing details, please contact R.D.T. at r.d.traub@bham.ac.uk.

Targeting Vector. The targeting vector was the YCplac22 shuttle vector containing a 21-kb *Not*I–*Sal*I fragment of a murine gene encoding the 67-kDa form of glutamic acid decarboxylase

Abbreviations: AMPA, α-amino-3-hydroxy-5-methyl-4-isoxazolepropionic acid; EPSP, excitatory postsynaptic potential; GABA, γ-aminobutyric acid; IPSC, inhibitory postsynaptic current; GAD67, 67-kDa form of glutamic acid decarboxylase; GluR-B, glutamate receptor B subunit; X-Gal, 5-bromo-4-chloro-3-indolyl β-D-galactoside.

[‖]To whom reprint requests should be addressed at: Max-Planck-Institut für Medizinische Forschung, Jahnstrasse 29, D-69120 Heidelberg, Germany. E-mail: monyer@mpimf-heidelberg.mpg.de.

The publication costs of this article were defrayed in part by page charge payment. This article must therefore be hereby marked "*advertisement*" in accordance with 18 U.S.C. §1734 solely to indicate this fact.

(GAD67), spanning parts of exon 1 up to intron 6 (about 19 kb downstream of the start codon) (11). The dicistronic GluR-B-IRES-lacZ cassette was introduced 30 bp upstream of the translational start codon of the GAD67 gene by using homologous recombination in yeast (12). The rat glutamate receptor B subunit (GluR-B) cDNA encoding the Q/R site edited in the flip configuration was used, and it contains 200 bp of the 5′ untranslated region (13). The flip variant of the GluR-B subunit was chosen because it endows the receptor with slower kinetic properties than the flop variant (13, 14). The IRES-lacZ cassette is described in Mountford *et al.* (15) and was cloned directly downstream of the GluR-B translational stop codon. The targeting vector was linearized at the unique *Not*I site, and after electroporation of embryonic stem cells (R1) (16), two positive clones were identified by Southern blot analysis with a 1.2-kb *Sal*I–*Not*I fragment as a probe, located directly upstream of the 5′ end of the targeting construct. Clone 18-5 was injected into C57BL6 blastocysts, and chimeric animals were backcrossed to C57BL6 mice. Anatomical and electrophysiological analyses were performed with heterozygous and wild-type littermates of F_2 and F_3 backcrosses to C57BL6.

5-Bromo-4-chloro-3-indolyl β-D-Galactoside (X-Gal) Staining. X-Gal staining was performed as previously described (17). Briefly, mice were transcardially perfused with 4% paraformaldehyde (PFA) in PBS. Brains were removed and postfixed in 4% PFA. Sections (50 μm) were cut on a Vibratome and incubated free-floating in X-Gal.

Immunocytochemistry. After X-Gal staining, the free-floating sections were incubated overnight at 4°C with a rabbit anti-GluR-B antibody (PharMingen, dilution 1:25) in 2% normal goat serum diluted in Tris-buffered saline (TBS), pH 7.4. After washing, the sections were incubated for 2 h at room temperature with a Texas red-conjugated anti-rabbit IgG secondary antibody (dilution: 1:100) (Jackson ImmunoResearch).

Electrophysiology. Transverse dorsal hippocampal slices (400 μm thick) were prepared from brains of male mice after decapitation following cervical dislocation, and maintained as described previously (6). Brief tetanic stimuli (100 Hz, 200 ms, 8–30 V, 50-μs duration) at threshold for evoking gamma oscillations were delivered simultaneously to the stratum radiatum proximal to the cell body layer at two recording sites at either end of the CA1 region (separation 0.7–1.1 mm) every 4 min throughout each experiment. Posttetanic oscillations were studied as field potentials recorded simultaneously by using glass micropipettes filled with 2 M NaCl (resistance 1–10 MΩ), at the level of stratum pyramidale at each site. Intracellular recordings were also taken from pyramidal cells and electrophysiologically identified fast-spiking stratum pyramidale interneurons by using electrodes filled with 2 M potassium methylsulfate or potassium acetate (resistance 50–90 MΩ).

Spontaneous EPSPs were recorded from fast-spiking stratum pyramidale interneurons in the presence of R-CPP (20 μM) and 2-OH-saclofen (0.1 mM). Cell membrane potential was kept at −70 mV throughout. Fast inhibitory postsynaptic potentials were not blocked, but no significant differences in fast inhibition were seen in the experimental groups used (see text).

IPSCs were recorded by using single electrode voltage clamp of pyramidal neurons in the presence of 2,3-dihydroxy-6-nitro-7-sulfamoylbenzo[*f*]quinoxaline (NBQX; 20 μM), R-CPP (20 μM), and 2-OH-saclofen (0.1 mM). In addition, recording pipettes contained 50 mM QX314 to block fast sodium spikes. Data were taken from 8 cells from five wild-type mice, 15 cells from three mice with a knock-in of Cre recombinase, and 13 cells from five mice with the knock-in of GluR-B. Conductance measurements were taken from IPSC responses stepped at 10 mV intervals between −80 mV and −40 mV holding potential.

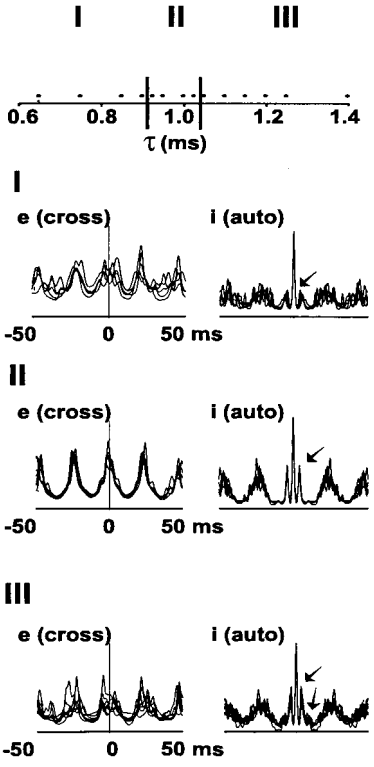

Fig. 1. Two-site synchronization occurs only over a narrow range of values for the decay time constant of interneuron AMPA-receptor-mediated EPSCs (simulations). Data are taken from 14 simulations, each with identical parameters, except for τ_{AMPA} (designated τ on the abscissa). The behavior of the system can be divided into three regimes: I, with $\tau \leq 0.9$ ms, having poor two-site synchrony; II, with 0.925 ms $\leq \tau \leq$ 1.025 ms, having good synchrony; III, with $\tau \geq 1.05$ ms, again with poor synchrony. In each regime, we plot superimposed cross-correlations of local average pyramidal cell voltages (e), from opposite ends of the array, using each simulation in that regime; and also superimposed autocorrelations of local average interneuron voltages (i), again using each simulation in the regime. In regimes I and III, the pyramidal cross-correlations lack a clear peak at 0 ms, and interneuron autocorrelation has either small, single side peaks (I), or double side peaks (III) (arrows). In regime II, in contrast, there is a sharp peak near 0 ms in the pyramidal cross-correlation, and single, sharp side peaks in the interneuron autocorrelation, the latter corresponding to synchronized interneuron doublet firing.

Results

In Network Simulations, the Time Course of EPSCs on Interneurons Must Be Relatively Precisely Tuned for Two-Site Synchrony to Occur, Whereas the Strength of IPSCs on Interneurons Is Expected to Be Less Critical. We first examined how synchronization in the model depended on the time course of unitary AMPA receptor-mediated EPSCs in interneurons, varying the parameter τ in the formula for a unitary EPSC: $2 \times t \times \exp(-t/\tau)$ nS (t = time after onset of the EPSC, in ms). Fig. 1 summarizes data from 14 such simulations. We show superimposed cross-correlations of local average pyramidal cell (e-cell) signals, taken from opposite ends of the array; and also autocorrelations of local average interneuron (i-cell) signals. The qualitative behavior of the network falls into three regimes, which we designate I, II, and III in the figure. In regime II, there is a single well-defined peak in the e-cell cross-correlation, near 0 ms, corresponding to synchrony of the oscillations. In regime II, the i-cell autocorrelation has two sharp side peaks at approximately ±4 ms, indicating precise

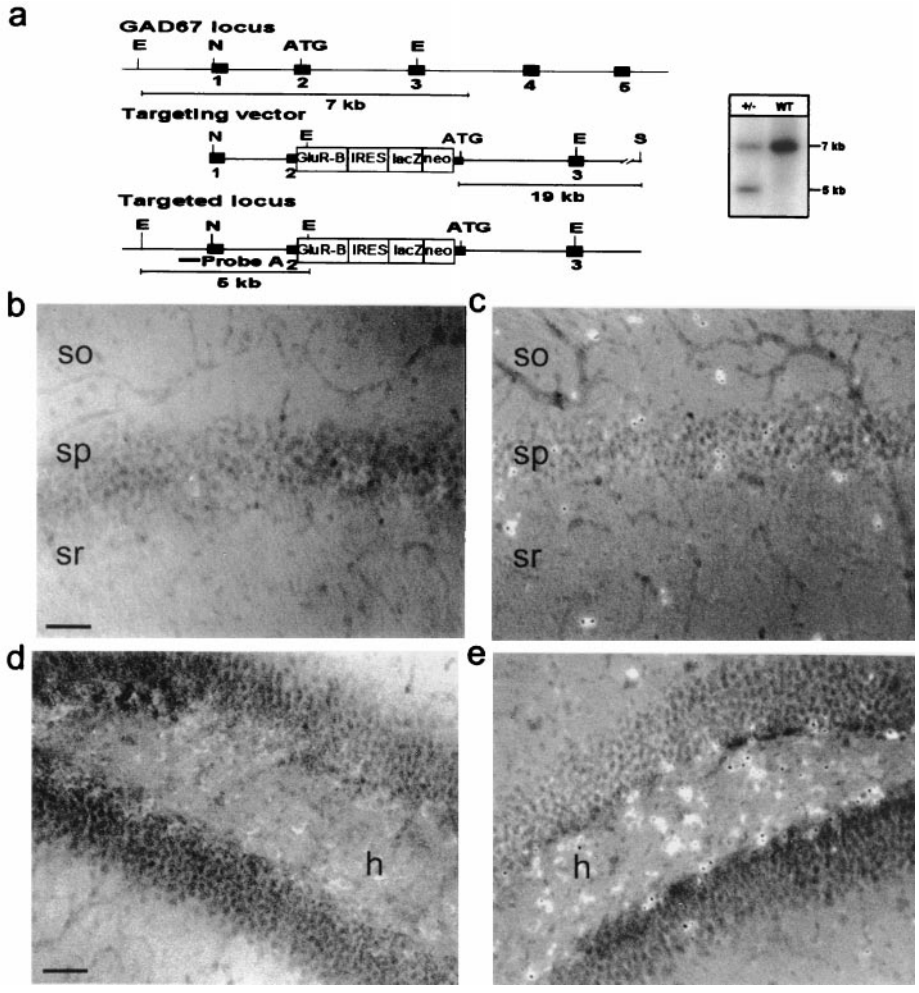

Fig. 2. Generation of mutant mice with elevated GluR-B expression in GABAergic interneurons. (*a*) Schematic representation of gene segments of the wild-type GAD67 allele, the targeting vector, and the targeted GAD67 allele. Positions of *Eco*RI (E), *Not*I (N), and *Sal*I (S) restriction sites are indicated. The PCR fragment used as probe for the Southern blot is indicated as a black bar. (*Right*) Southern blot analysis of tail DNA isolated from wild-type and heterozygous mice, digested with *Eco*RI to distinguish wild-type (7-kb) and targeted (5-kb) alleles. (*b–e*) GluR-B immunostaining in wild-type (*b* and *d*) and combined immunostaining and X-Gal staining in the mutant (*c* and *e*) hippocampus. Note the much higher GluR-B expression in LacZ-positive GABAergic interneurons compared with neighboring pyramidal cells in the mutant CA1 region (*c*) and hilus (e). This expression was never seen in the corresponding areas in control animals (*b* and *d*). (Scale bars, 100 μm.) so, Stratum oriens; sp, stratum pyramidale; sr, stratum radiatum; h, hilus. For higher magnification see Fig. 6 in the supplemental data.

timing of interneuron doublets. Regime II corresponds to values of τ between 0.925 and 1.025 ms, an approximately 10% variation. With τ outside this relatively narrow range, either too small or too large, two-site synchrony is degraded, as indicated by the breadth around 0, and multiple peaks, in the e-cell cross-correlations (regimes I and III in Fig. 1). Correspondingly, the i-cell autocorrelation is altered. In regime I, the side peaks (arrows) are smaller than in regime II, signifying the occurrence of fewer doublets when τ is too small (i.e., when interneuron EPSCs are somewhat smaller and faster). In regime III, additional side peaks (arrows) occur in the interneuron autocorrelation, indicating the existence of triplet firing, a consequence of the somewhat larger and more prolonged interneuron EPSCs.

Fig. 1 implies that in our network model, stable two-site synchrony occurs over a relatively narrow range of values of τ, and small changes in this parameter are predicted—in the biological system—to degrade two-site synchronization. We used molecular techniques to force the biological system from regime II into regime III.

The model also makes predictions about the firing patterns of the neurons, as synchrony becomes degraded. This is shown in Fig. 5 (which is published as supplemental data on the PNAS web site, www.pnas.org), where we illustrate further details from representative simulations selected from Fig. 1, one simulation from each regime.

Generation of a Mouse Line with Overexpression of GluR-B AMPA Receptor Subunit in GABAergic Interneurons. Major determinants of EPSP duration are electrotonic properties, including the location of the synaptic contacts, and AMPA receptor kinetics. Low expression of the GluR-B subunit in GABAergic interneurons is one of the molecular bases for faster EPSPs/EPSCs in many synapses (18–24) (for review see ref. 25). Hence, we overexpressed the GluR-B subunit in GABAergic interneurons of the mouse, to prolong EPSPs in these cells.

To accomplish this, we generated mutant mice in which the rat cDNA for GluR-B was targeted into an endogenous GAD67 allele by using homologous recombination in embryonic stem cells (Fig. 2*a*). To facilitate the analysis of the mutant mice, the targeting vector was designed such that the GAD67 gene-targeted GluR-B cDNA is followed by an IRES-lacZ cassette (15). Because the knock-out of both GAD67 alleles is lethal (26), mice heterozygous for the altered GAD67 allele were used in this study. These heterozygous mutant mice exhibited normal growth

and reproductive behavior, and the brain showed no obvious abnormalities to macroscopic and histological examination. The animals were seizure-free.

The targeted insertion of the dicistronic GluR-B-IRES-lacZ construct into the GAD67 allele did not alter the expression characteristics of the GAD67 gene, as demonstrated by the specific X-Gal staining in a subpopulation of neurons, the putative GABAergic interneurons (not shown). LacZ-mediated staining could clearly be identified in populations of neurons known to be primarily GABAergic, including neurons of the nucleus reticularis thalami, the septal nucleus, the inferior and superior colliculus, the ventral lateral geniculate nucleus, the Purkinje cells, and putative Golgi and stellate cells of the cerebellum (not shown) (27, 28). The GAD67 promoter-controlled restricted expression of the dicistronic construct in interneurons was also confirmed by double-labeling experiments, which showed that X-Gal staining occurred only in GAD67-positive cells (not shown).

Immunocytochemistry revealed elevated GluR-B expression in GABAergic interneurons. In fact, in the mutant, the highest level of GluR-B is found in GABAergic interneurons (Fig. 2 *c* and *e*), in contrast to wild type, where GluR-B expression in this cell population is low (Fig. 2 *b* and *d*; see also Fig. 6, which is published as supplemental data on the PNAS web site, www.pnas.org).

As a further control, we also used a mouse line in which Cre recombinase had been inserted in the same locus as the GluR-B-IRES-lacZ cassette, 30 bp upstream of the translational start codon of the GAD67 gene. These mice were used to test for nonspecific effects of the genetic manipulations on synaptic inhibition, as well as on cell-firing and oscillation patterns.

Interneuronal EPSPs, and the Local Synchrony and Two-Site Synchrony of Tetanically Elicited Gamma Oscillations, in Mutant Mice as Compared with Wild-Type Mice. Loss of one functional GAD67 allele, in heterozygous mice, and in Cre-recombinase-inserted mice, did not affect inhibitory neurotransmission. Monosynaptic pharmacologically isolated IPSCs from pyramidal cells showed no significant difference in conductance, decay constant, or reversal potential between each of the three groups (wild-type values 127 ± 12 nS, 8 cells from five animals; GAD-Cre mutant values 135 ± 22 nS, 15 cells from three animals; GAD-GluR-B mutant values 129 ± 16 nS, 13 cells from five animals; $P > 0.05$). These measurements do not take into account any possible effects of depletion of GABA stores. However, measurement of the mean amplitude of inhibitory postsynaptic potentials (IPSPs) in the train underlying the posttetanic gamma oscillations also showed no significant difference, although the amplitude of IPSPs in any given posttetanic gamma response varied much more in GluR-B mutant mice than in wild-type mice (Fig. 3*c*). Specific values were as follows: wild-type, 1.8 ± 0.3 mV; GluR-B mutant, 2.1 ± 0.7 mV ($P > 0.05$). The effects of subtle alterations of tetanically elicited gamma oscillations, induced by subtle alterations in IPSCs in interneurons alone, are not known experimentally; the network model, however, suggests that oscillatory behavior is not sensitive to this parameter (Fig. 7, which is published as supplemental data on the PNAS web site, www.pnas.org).

Interneuronal properties and network oscillations were studied with simulations (as illustrated above) and with electrophysiological techniques (5, 6). Analysis of spontaneous AMPA receptor-mediated EPSPs seen in 2-min epochs of data from five wild-type and five mutant mice showed prolonged rise and decay times (Fig. 3*a*). Although little difference was seen in the mean values of these measurements, a significantly larger number of longer slower-to-peak EPSPs was seen in the mutant ($P < 0.05$, two-way nonparametric ANOVA). Single-shock stimulation (5–20 V) of stratum oriens or stratum radiatum in wild-type mice elicited either EPSPs alone or EPSPs leading to a single action

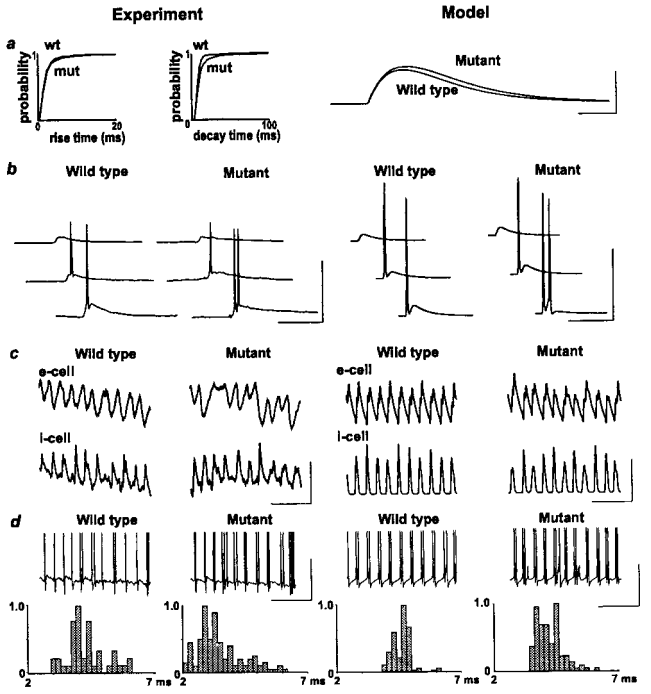

Fig. 3. Firing properties of interneurons are altered by genetically manipulated overexpression of GluR-B. (*a*) Spontaneous EPSP rise time and decay time plots for stratum pyramidale fast-spiking interneurons, recorded from a membrane potential of −70 mV. Data are shown as cumulative probability for >4,000 EPSPs from five cells from five wild-type and five cells from five mutant mice. Model data show change in unitary EPSC for parameters that best fit the experimental data: ''wild-type'' unitary EPSC = $t \exp(-t/0.95)$ nS, ''mutant'' unitary EPSC = $t \exp(-t/1.05)$ nS. (Scale bars: 0.8 nS, 1 ms.) (*b*) Firing pattern in response to a single proximal stratum radiatum stimulation. Traces show response (from −70 mV) to increasing stimulus intensity (5–20 V) for interneurons from wild-type and mutant. Note increasing intensities generate double spikes in the cell from the mutant. (Scale bars: 50 mV, 40 ms.) Model data show voltage responses for single interneurons (holding current −0.165 nA) receiving identical EPSC onto single compartments on each of three dendrites. Each EPSC had the time course $ct \exp(-t/\tau)$, where $\tau = 0.95$ for control and 1.05 for mutant; $c = 16.1, 47.4, 83.8$ nS (top to bottom). Note the spike doublet in the mutant, but not in the wild type (as in experiment). (Scale bars: 50 mV, 30 ms.) (*c*) Pattern of pyramidal cell phasic inhibitory input (upper traces) and interneuron phasic excitatory input (lower traces) during posttetanic oscillations, in wild-type and in mutant mice. The interneuron was hyperpolarized by injection of −0.2 nA current. [Scale bars (experiment): 2 mV, 100 ms.] Model data show $GABA_A$ conductance to an e-cell (upper traces) and AMPA conductance to an i-cell. Note, in the ''mutant,'' the more variable amplitude of $GABA_A$ inputs, and the variable width of the AMPA inputs. [Scale bars (model): 150 nS, 100 ms.] (*d*) Example traces of interneuron firing patterns during gamma-frequency oscillations following paired tetanic stimulation, illustrating the increased incidence of doublet formation and the occurrence of occasional spike bursts. Model data show voltage of a selected interneuron from network simulations in the wild type and the mutant. The only difference in parameters for these simulations was in interneuron EPSC time course illustrated in *a*. [Scale bars (experiment and model): 20 mV, 100 ms.] Below are histograms illustrating the probability of a doublet of interval *x* relative to the sample mode. There are 45 doublets from wild-type data (n = three cells from three animals) and 130 doublets from mutant data (n = five cells from five animals). Model histograms were constructed by using ≈110 doublet intervals for simulations of ''wild type'' and ''mutant'' gamma oscillations, each pooled from seven interneurons.

potential, whereas single stimulations (5–20 V) in the mutant elicited EPSPs with spike doublets at intensities more than 10 V. The incidence of doublets when single shock stimulation was used was wild-type, 0/5 cells each from one mouse; mutant, 6/6 cells from five mice (data not shown). In simulations, small

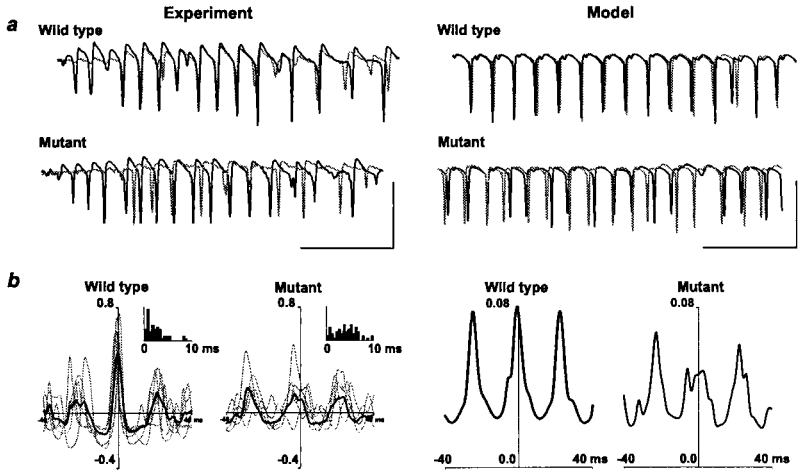

Fig. 4. Population gamma oscillations have disrupted synchrony in the mutant mice. (*a*) Example traces. Paired stratum pyramidale field potential recordings illustrated from the beginning of the posttetanic oscillatory response induced by paired tetanic stimulation. Recording site separation ≈1 mm along the CA1 axis. Recordings are overlaid to illustrate temporal relationship between population spikes at the two sites. Oscillations from the mutant mice show a more erratic temporal relationship between spike generation at each site. (Scale bars: 3 mV, 100 ms.) Model data show superimposed average voltage signals, from two ends of the model array, for the two simulations (wild type and mutant). Each average was of 224 somatic pyramidal cell potentials, and the signals are inverted so as to resemble the experimental field potentials. Note the tight synchrony in the wild type, contrasted with the jittering back and forth in the mutant. (Scale bars: 50 mV, 100 ms.) (*b*) Pooled data showing pattern of phase relationship change in the mutant mice. Cross-correlations are taken from data as in *a*. Control data show mean cross-correlation plot for data from each of six wild-type mice (gray curves) and the global mean from these plots (black line). *Inset* shows distribution of modular phase relationships for 62 paired posttetanic gamma oscillations from 11 slices from six wild-type animals. Cross-correlation data from slices from mutant mice are represented in the same manner ($n = 5$ mice). Note erratic nature of central peak amplitudes. *Inset* shows distribution of modular phase relationships from 74 posttetanic oscillations from 15 slices from five mice. Model data show cross-correlations of 200 ms of data from the average signals shown in *a*.

increases in the time course of EPSC kinetics alone, using a multicompartment interneuron model (29), gave similar results (data not shown).

Interneurons from wild-type mice, recorded during two-site stimulated gamma oscillation, fired in a pattern of single spikes and spike doublets, as reported previously for rats (4, 6). In contrast, interneurons from the mutant mice fired in doublets and triplets during gamma oscillations (Fig. 3*c*). Analysis of doublet intervals showed a median interval of 4.2 (3.8–4.8) ms in slices from wild-type mice and 3.3 (2.9–4.7) ms in the mutant mice ($P < 0.05$, two-way nonparametric ANOVA). Network simulations of gamma oscillations were run, using the model of 3,072 pyramidal neurons and 384 interneurons used above. The "wild-type" simulation was from region II of Fig. 1 (τ_{AMPA} = 0.95 ms), and the "mutant" simulation was from the left-most portion of region III (τ_{AMPA} = 1.05 ms). Thus, "wild-type" and "mutant" simulations differed only in the slightly different time courses of interneuron EPSCs, as shown in Fig. 3*a*. The simulations exhibited the same patterns of interneuronal firing as observed in the experiments: singlets and doublets in wild type, doublets and triplets in the mutant. As in the experimental recordings, "mutant" doublet intervals were shortened, in simulations, compared with "wild-type" doublet intervals [wild-type median interval 4.7 (4.3–4.9) ms, mutant median interval 4.1 (3.7–4.6) ms, $P < 0.05$ Mann–Whitney test].

Two-site stimuli, in the CA1 region of hippocampal slices from wild-type mice, elicited gamma oscillations that were synchronized between sites on a millisecond time scale (Fig. 4*a*), as previously observed in rat hippocampal slices (4–6). In contrast, two-site synchrony was disrupted in slices from the mutant mice. Inspection of superimposed field potential traces from the two sites indicated that the loss of synchrony is reflected in time-varying phase lags between the sites (Fig. 4*a*), and not by differences in mean frequency between the two sites. Exactly this pattern was observed in network simulations, using the same manipulation of interneuron EPSP time course illustrated in Fig. 3*a* (and Fig. 5*a* in the supplemental data). Synchrony was robust in wild-type mice, with a median phase difference between sites of 1.9 (1.0–3.0) ms (Fig. 4*b*, *Inset*); in the mutant mice, synchrony was significantly less precise, with a median phase difference between sites of 4.4 (2.0–7.0) ms ($P < 0.05$, two-way nonparametric ANOVA). A similar detrimental effect on long-range synchrony was observed in cross-correlograms from simulations, including the prolonged EPSP time course illustrated in Fig. 3*a*. As determined by these simulations, phase variations were caused by the triplet firing of interneurons at one site, combined with doublet firings at the other site. Disruption in synchrony was not caused by differences in mean frequency between the two ends of the array: in the control simulation, the left and right sides of the array had mean frequency (determined by the first rightward peak in the autocorrelation) of 42.4 and 39.5 Hz, respectively; in the "mutant" simulation, the autocorrelations exhibited multiple peaks, caused by the variable oscillation intervals, but the main peaks corresponded to 53.2 Hz and 53.8 Hz for the two sides, respectively.

Discussion

Here we show how the firing of spike doublets with precise interspike intervals acts to stabilize synchrony between two oscillating neuronal sites and that synchrony is critically determined by EPSP kinetics in interneurons.

AMPA receptor-mediated currents rise and decay faster in interneurons than in principal neurons, in part because of different subunit profiles (30–32). Electrophysiological studies indicate that, in hippocampus, pyramidal/interneuron synaptic connections are powerful and elicit action potentials at short latency, even in resting conditions, when only one or a few presynaptic cells fire (19, 24). Hence, such synaptic connections have the properties desired for providing precise timing information.

In the mutant mice described here, whose interneurons express a larger-than-usual content of GluR-B, pyramidal/

interneuron connections are more powerful (larger and/or longer AMPA receptor-mediated synaptic currents); indeed, single shocks elicit double action potentials in the mutant interneurons, but only single spikes in wild-type, over the range of stimulus intensities that we investigated. The network consequence of this enhanced synaptic excitability of the mutant interneurons is that, during tetanically elicited gamma oscillations, the second spike of each doublet is more likely to be generated as a consequence of the enhanced local excitation and thus contains no temporal information required to adjust long-range synchrony. In addition, interneurons in the mutant fire triplets as well as doublets and thus, as predicted by our model (9) (Fig. 1), two-site synchrony of gamma oscillations is disrupted. Evidently, excessive firing of interneurons interferes with the precision of the feedback signals necessary to sustain synchrony. Note, however, that interneuron triplet firing *per se* need not necessarily disrupt synchrony, either experimentally during beta (10- to 25-Hz) oscillations (5) or in models (33).

Disruption of synchrony in these experiments was induced by overexpression of the GluR-B subunit in GABAergic interneurons. Whereas a minority of GABAergic interneurons express GluR-B at levels comparable with pyramidal cells (34), in most GABAergic interneurons this subunit is expressed at significantly lower levels. This expression pattern has been documented by *in situ* hybridization (35–37) and immunocytochemistry (34, 38–41). Low GluR-B expression in GABAergic cells affects a number of AMPA receptor properties, including Ca^{2+} permeability (31, 32, 42, 43), block by polyamines (44), and single-channel conductance (22), and is the molecular basis for certain novel forms of plasticity (44–46). Although GluR-B incorporation into heteromeric AMPA receptors affects other parameters in addition to kinetics, our experimental and modeling data indicate that the slowing of EPSPs is the principal factor by which overexpression of GluR-B in GABAergic interneurons disrupts oscillation synchrony.

In summary, our data suggest that the rapid kinetics of AMPA receptors in interneurons could be serving a distinct neurophysiological purpose: to allow precise synchronization of gamma oscillations over long distances.

We thank Peter Seeburg and Bard Ermentrout for helpful discussions. This work was supported by grants from the Deutsche Forschungsgemeinschaft (SFB 317) and the Schilling Foundation to H.M., from the Wellcome Trust to R.D.T. and M.A.W., and from the National Science Foundation to N.K. R.D.T. is a Wellcome Principal Research Fellow. E.C.F. was supported by the Graduate Program of Molecular and Cellular Neurobiology of the University of Heidelberg.

1. Singer, W. & Gray, C. M. (1995) *Annu. Rev. Neurosci.* **18,** 555–586.
2. Murakoshi, T., Guo, J. Z. & Ichinose, T. (1993) *Neurosci. Lett.* **163,** 211–214.
3. Aroniadou, V. A. & Keller, A. (1993) *J. Neurophysiol.* **70,** 1553–1569.
4. Traub, R. D., Whittington, M. A., Stanford, I. M. & Jefferys, J. G. (1996) *Nature (London)* **383,** 621–624.
5. Traub, R. D., Whittington, M. A., Buhl, E. H., Jefferys, J. G. & Faulkner, H. J. (1999) *J. Neurosci.* **19,** 1088–1105.
6. Whittington, M. A., Stanford, I. M., Colling, S. B., Jefferys, J. G. & Traub, R. D. (1997) *J. Physiol. (London)* **502,** 591–607.
7. Bibbig, A. (2000) Ph.D. thesis (Universität Ulm, Ulm, Germany).
8. Ermentrout, G. B. & Kopell, N. (1998) *Proc. Natl. Acad. Sci. USA* **95,** 1259–1264.
9. Whittington, M. A., Traub, R. D., Faulkner, H. J., Jefferys, J. G. & Chettiar, K. (1998) *Proc. Natl. Acad. Sci. USA* **95,** 5807–5811.
10. Martina, M., Vida, I. & Jonas, P. (2000) *Science* **287,** 295–300.
11. Szabo, G., Katarova, Z., Kortvely, E., Greenspan, R. J. & Urban, Z. (1996) *DNA Cell. Biol.* **15,** 1081–1091.
12. Storck, T., Kruth, U., Kolhekar, R., Sprengel, R. & Seeburg, P. H. (1996) *Nucleic Acids Res.* **24,** 4594–4596.
13. Sommer, B., Keinanen, K., Verdoorn, T. A., Wisden, W., Burnashev, N., Herb, A., Kohler, M., Takagi, T., Sakmann, B. & Seeburg, P. H. (1990) *Science* **249,** 1580–1585.
14. Mosbacher, J., Schoepfer, R., Monyer, H., Burnashev, N., Seeburg, P. H. & Ruppersberg, J. P. (1994) *Science* **266,** 1059–1062.
15. Mountford, P., Zevnik., B., Duwel., A., Nichols, J., Li, M., Dani, C., Robertson, M., Chambers, I. & Smith, A. (1994) *Proc. Natl. Acad. Sci. USA* **91,** 4303–4307.
16. Nagy, A., Rossant, J., Nagy, R., Abramow-Newerly, W. & Roder, J. C. (1993) *Proc. Natl. Acad. Sci. USA* **90,** 8424–8428.
17. Bonnerot, C. & Nicolas, J. F. (1993) *Methods Enzymol.* **225,** 451–469.
18. Miles, R. (1990) *J. Physiol. (London)* **428,** 61–77.
19. Gulyas, A. I., Miles, R., Sik, A., Toth, K., Tamamaki, N. & Freund, T. F. (1993) *Nature (London)* **366,** 683–687.
20. Hestrin, S. (1993) *Neuron* **11,** 1083–1091.
21. Buhl, E. H., Halasy, K. & Somogyi, P. (1994) *Nature (London)* **368,** 823–828.
22. Geiger, J. R., Lübke, J., Roth, A., Frotscher, M. & Jonas, P. (1997) *Neuron* **18,** 1009–1023.
23. Ali, A. B., Deuchars, J., Pawelzik, H. & Thomson, A. M. (1998) *J. Physiol. (London)* **507,** 201–217.
24. Csicsvari, J., Hirase, H., Czurko, A. & Buzsaki, G. (1998) *Neuron* **21,** 179–189.
25. Geiger, J. R. P., Roth, A., Taskin, B. & Jonas, P. (1999) in *Ionotropic Glutamate Receptors in the CNS*, Handbook of Experimental Pharmacology, eds. Jonas, P. & Monyer, H. (Springer, Berlin), Vol. 141, pp. 363–398.
26. Asada, H., Kawamura, Y., Maruyama, K., Kume, H., Ding, R. G., Kanbara, N., Kuzume, H., Sanbo, M., Yagi, T. & Obata, K. (1997) *Proc. Natl. Acad. Sci. USA* **94,** 6496–6499.
27. Erlander, M. G., Tillakaratne, N. J., Feldblum, S., Patel, N. & Tobin, A. J. (1991) *Neuron* **7,** 91–100.
28. Esclapez, M., Tillakaratne, N. J., Kaufman, D. L., Tobin, A. J. & Houser, C. R. (1994) *J. Neurosci.* **14,** 1834–1855.
29. Traub, R. D. & Miles, R. (1995) *J. Comput. Neurosci.* **2,** 291–298.
30. Angulo, M. C., Lambolez, B., Audinat, E., Hestrin, S. & Rossier, J. (1997) *J. Neurosci.* **17,** 6685–6696.
31. Jonas, P., Racca, C., Sakmann, B., Seeburg, P. H. & Monyer, H. (1994) *Neuron* **12,** 1281–1289.
32. Geiger, J. R., Melcher, T., Koh, D. S., Sakmann, B., Seeburg, P. H., Jonas, P. & Monyer, H. (1995) *Neuron* **15,** 193–204.
33. Karbowski, J. & Kopell, N. (2000) *Neural Comput.* **12,** 1573–1606.
34. Leranth, C., Szeidemann, Z., Hsu, M. & Buzsaki, G. (1996) *Neuroscience* **70,** 631–652.
35. Catania, M. V., Tolle, T. R. & Monyer, H. (1995) *J. Neurosci.* **15,** 7046–7061.
36. Catania, M. V., Bellomo, M., Giuffrida, R., Stella, A. M. & Albanese, V. (1998) *Eur. J. Neurosci.* **10,** 3479–3490.
37. Racca, C., Catania, M. V., Monyer, H. & Sakmann, B. (1996) *Eur. J. Neurosci.* **8,** 1580–1590.
38. Vissavajjhala, P., Janssen, W. G., Hu, Y., Gazzaley, A. H., Moran, T., Hof, P. R. & Morrison, J. H. (1996) *Exp. Neurol.* **142,** 296–312.
39. Kondo, M., Sumino, R. & Okado, H. (1997) *J. Neurosci.* **17,** 1570–1581.
40. Petralia, R. S., Wang, Y. X., Mayat, E. & Wenthold, R. J. (1997) *J. Comp. Neurol.* **385,** 456–476.
41. He, Y., Janssen, W. G., Vissavajjhala, P. & Morrison, J. H. (1998) *Exp. Neurol.* **150,** 1–13.
42. Lambolez, B., Ropert, N., Perrais, D., Rossier, J. & Hestrin, S. (1996) *Proc. Natl. Acad. Sci. USA* **93,** 1797–1802.
43. Toth, K. & McBain, C. J. (1998) *Nat. Neurosci.* **1,** 572–578.
44. Rozov, A. & Burnashev, N. (1999) *Nature (London)* **401,** 594–598.
45. Gu, J. G., Albuquerque, C., Lee, C. J. & MacDermott, A. B. (1996) *Nature (London)* **381,** 793–796.
46. Mahanty, N. K. & Sah, P. (1998) *Nature (London)* **394,** 683–687.